Pre-crystallization heat treatment and infrared luminescence enhancement in Ni^{2+}-doped transparent glass-ceramics

N.V. Golubev*[1], E.S. Ignat'eva[1], V.M. Mashinsky[2], E.O. Kozlova[1], V.N. Sigaev[1], A. Monguzzi[3], A. Paleari[1,3], R. Lorenzi[3]

[1]P.D. Sarkisov International Laboratory of Glass-based Functional Materials, Mendeleev University of Chemical Technology of Russia, 9 Miusskaya Square, 125047 Moscow, Russia. E-mail: golubev_muctr@mail.ru

[2]Fiber Optics Research Center, Russian Academy of Sciences, 38 Vavilov Str., 119333 Moscow, Russia

[3]Department of Materials Science, University of Milano-Bicocca, via Cozzi 55, 20125 Milano, Italy

Abstract

We report on design and fabrication of Ni^{2+}-doped glass-ceramics from a low-alkali optical glass in Li_2O-Na_2O-Ga_2O_3-SiO_2-GeO_2 system by melting technique and subsequent thermally controlled nano-crystallization. The analysis of differential scanning calorimetry, X-ray diffraction, transmission electron microscopy, absorption and fluorescence spectroscopy reveals, for the first time, the real possibility of optimizing the integrated intensity of Ni^{2+} near-infrared emission through controlled pre-treatments at temperatures of nanophase nucleation, with the enhancement up to a factor of four with respect to gallium germanosilicate glass-ceramics obtained without pre-treatments. Importantly, the effects on the light emission are shown to be related to the influence of pre-treatment on size and size distribution of the gallium oxide nanocrystals which result from subsequent crystallization at higher temperature.

Keywords: glass-ceramics, luminescence, nucleation, crystallization, nanocrystals, Ga_2O_3

1. Introduction

Pre-crystallization heat treatment is known to have strong influence on subsequent crystallization and final properties of glass-ceramics [1]. Nevertheless, most studies on the effects of heat treatments on the structure and properties of multi-component glass-ceramics are aimed at the investigation of phase transformation during glass crystallization, revealing structure and property changes just at the crystallization range. In particular, only one-step isothermal treatment is used for Ni^{2+}-doped low-alkali gallium silicate glasses to fabricate glass-ceramics [2-19], with the exception of one paper where two-step heat treatment [20] was applied for few glass compositions but without any investigation of luminescence efficiency as a function of such treatment. Moreover, the effect of heat treatment conditions on the luminescence efficiency (quantum yield or integrated intensity of the luminescence band), which is one of the target characteristics of the final material, has received no attention in previous papers on Ni^{2+}-doped low-alkali gallium silicate glasses [2-20].

The interest in Ni^{2+}-doped silicate glass-ceramics stems from their broadband near-infrared (NIR) emission coupled with the ease of fiber drawing and lower production cost relative to crystals. Such materials are considered to be promising for the use as broadband optical gain media [11, 13], in spite of the strong excited absorption of Ni^{2+} [21], and are investigated as potential solutions for strategies of substitution of critical raw materials like rare earth doped compounds. However, high melting temperature required to prepare low-alkali gallium silicate glasses substantially hinders their fabrication and leads to poor optical quality of the initial glass [22]. In contrast, low-alkali gallium germanosilicates can be obtained at temperatures lower than 1500 ºC and after doping with Ni^{2+} also demonstrate broadband NIR emission with comparable quantum yield [23-25]. Two-step heat treatment of Ni-free low-alkali gallium germanosilicates was shown to have notable impact on size and number of nanocrystals (NCs) of spinel-like gallium oxide precipitated in the glass matrix [26]. In regard to Ni^{2+}-doped germanosilicates, only one-step heat treatment has been used up to now, and a strong correlation has been revealed between the number of Ni^{2+} ions per NC and the integrated intensity of the related broadband NIR emission [24]. For this reason, pre-crystallization heat treatment seems to be a powerful tool to enhance the efficiency of Ni^{2+} luminescence in the germanosilicate glass-ceramics by controlling the sub-microstructure of the material.

In this paper we shed further light on the complex correlation between early stage of phase separation and luminescence efficiency of Ni^{2+}-doped glass-ceramics. The main objective was to develop two-step heat treatment regime and to study efficiency of Ni^{2+} luminescence as a function of pre-crystallization heat treatment, with the aim of increasing broadband NIR emission from transparent Ni^{2+}-doped glass-ceramics.

2. Experimental

The present work has been carried out on stria-free glass from a single melt obtained in ~250 ml platinum crucible. Glass with nominal composition $7.5Li_2O$-$2.5Na_2O$-$20Ga_2O_3$-$35GeO_2$-$35SiO_2$ doped with 0.1 NiO (mol%) was prepared using special purity grade amorphous SiO_2 (Ltd "Lanthan center for technology", Moscow, Russia), GeO_2 (JSC "Germanium", Krasnoyarsk, Russia), chemically pure Li_2CO_3 and Ga_2O_3 (Ltd "Rare Metals Plant", Koltsovo, Russia), Na_2CO_3 and NiO (Ltd "JSC Reachem", Moscow, Russia). Appropriate proportions of the raw materials were calculated in order to prepare 430 g of final product. The starting materials were weighed with an accuracy of 0.001 g and were dry mixed for 5 h before melting at 1480 °C for 2 h in a home-made electrically heated furnace. To increase melt homogeneity, oxygen bubbling through the molten glass was carried out by means of a platinum tube. After homogenization for 40 min, the melt was kept at 1480 °C for 5 min before casting into an unheated steel mould. The cast glass was then annealed in a muffle furnace (Termokeramica, Russia) heating from room temperature up to 520 °C at a rate of 10 °C/min, holding for 2 h and then cooling for 170 ºC, at ~14 ºC/h. The furnace was then turned off, and the glass was allowed to cool slowly to room temperature overnight. Square rods about 10×0.5×0.5 cm in size were cut from the resulting glass (hereafter, the "parent glass"). This material was used for all subsequent experiments aimed at revealing the effect of pre-crystallization temperatures on Ni^{2+} luminescence integrated intensity and the level of its enhancement that can be reached in two-step treated glasses compared with one-step treated reference sample.

One of the rods was cut into smaller samples, ~0.5×0.5×0.5 cm in size, and isothermally treated for different times. These samples were used to study the dependence of the nucleation process on the duration of pre-crystallization heat treatments by Marotta's method [27]. This method was

used as it can more accurately predict the temperature dependence of the nucleation rate rather than the peak height method in the case of considerable overlapping of the nucleation and growth processes [28]. The heat treatments were performed by placing the samples into the muffle furnace at room temperature, heating them at a rate of 10 °C/min up to 595 ºC (accuracy ±2 ºC) and holding for 2.5, 3.5, 4.5, 6.5 or 8.5 h. The treatment temperature was chosen according to previous data on similar glass indicating the occurrence of nucleation process in that range of temperatures [26].

Three other rods were used to reveal the influence of pre-crystallization heat treatments on luminescence efficiency of the glass-ceramics. The rods were placed in a hand-made gradient furnace and treated for 3.5 h at temperatures near T_g, in the range 550-630 ºC, where the highest nucleation rate is expected to occur [29]. Sections of one of these rods were cut from different parts along the rod length and were used for differential scanning calorimetry (DSC) analysis. The other two pretreated rods and a reference sample of the parent glass were then treated at 640 ºC for 15 min. Higher temperatures or longer duration led to increased light scattering of glass-ceramics obtained by one-step treatment compared with the glass heat treated in two steps. One of the two double treated rods was polished for optical measurements. Sections of the other rod were cut from different parts along the rod length and ground for X-ray diffraction (XRD) and transmission electron microscopy (TEM) analyses.

DSC measurements were performed by means of a thermal analyzer STA 449 F3 Jupiter (Netzsch, Germany) in platinum crucibles, at a heating rate of 10 ºC/min in Ar, on bulk samples of 22 ± 0.5 mg. The glass transition temperature (T_g) was determined as the extrapolated onset of the transition, while crystallization temperatures were defined as peak extremum temperatures in the DSC curves. Crystallization temperatures were reproducible to within ±1 ºC for several samples from the same melt confirming high homogeneity of the parent glass.

Optical absorption spectra were collected using a spectrophotometer UV-3600 (Shimadzu, Japan). Photoluminescence (PL) spectra in the NIR range were obtained with the help of optical spectrum analyzer AQ-6315A (Ando, Japan) upon excitation by a 966 nm hand-made source on the basis of a semiconductor laser diode. The diameter of the spot of exciting radiation on the samples was

~300 μm. Silica core optical fiber of 660 μm in diameter was used for collecting and guiding the PL light to the spectrum analyzer. The uncertainty of the relative PL intensity from light collection reproducibility is less than 10%. The integrated PL intensities after background subtraction were computed with the trapeze method for all glass-ceramic samples and were compared to evaluate luminescence enhancement. PL decay kinetics data have been collected in photon-counting mode using a L900 Flash Photolysis setup (Edinburgh Instruments, UK) coupled to an InGaAs photodiode detector (Hamamatsu Photonics, Japan), with a temporal resolution <2 ns and an uncertainty of about 10%. The excitation source employed is a Minilite II Continuum Nd:YAG pulsed laser (Photonic Solutions, UK) at 1064 nm with a pulse duration of 5 ns. PL decay kinetics was investigated integrating radiation at 1400 nm with a bandwidth of 20 nm. Convolution procedure was applied to the decay curves to determine PL lifetimes in double exponential fitting.

XRD patterns of powdered samples were recorded by means of a diffractometer D2 Phaser (Bruker, Germany) employing nickel-filtered CuKα radiation. Crystalline phases were identified by comparing the peak position and relative intensities in the X-ray diffraction pattern with the ICDD PDF-2 database. The crystallized fraction was estimated as $100 \cdot (A_p/A_x)$, where A_x and A_p are, respectively, the area of the whole XRD pattern (without background) and the area of the peaks considered as the area outside of the broad amorphous XRD pattern. Indicated areas were computed (in cps×degrees) with the trapeze method using DIFFRAC.EVA software.

TEM images and electron diffraction patterns were obtained on finely ground powder using a microscope JEM-2100 (JEOL, Japan) with an accelerating voltage of 200 kV. No effect of electron irradiation on the samples was observed during low-resolution TEM study. Measurements of 170-300 crystallites were made from various regions of the sample to establish NCs size distribution in fabricated glass-ceramics.

3. Results and discussion

3.1 Pre-treatment effects on the crystallization process

The influence of temperature (or time) of the pre-crystallization heat treatment on the process of bulk nucleation of the nanophase can be evaluated by the method developed by Marotta et al. [27]. In this technique, the difference, ΔT, between the peak crystallization temperature of the initial glass and pretreated samples is plotted against the temperature (or time) of the pre-crystallization heat treatment. The occurrence of efficient nucleation is registered by a maximum in ΔT *vs* temperature of pre-crystallization heat treatment. Furthermore, collecting data of ΔT in samples pretreated for different times at nucleation temperature, one can plot ΔT *vs* treatment time that reflects the rate of increase of the number density of nuclei during the heat treatment.

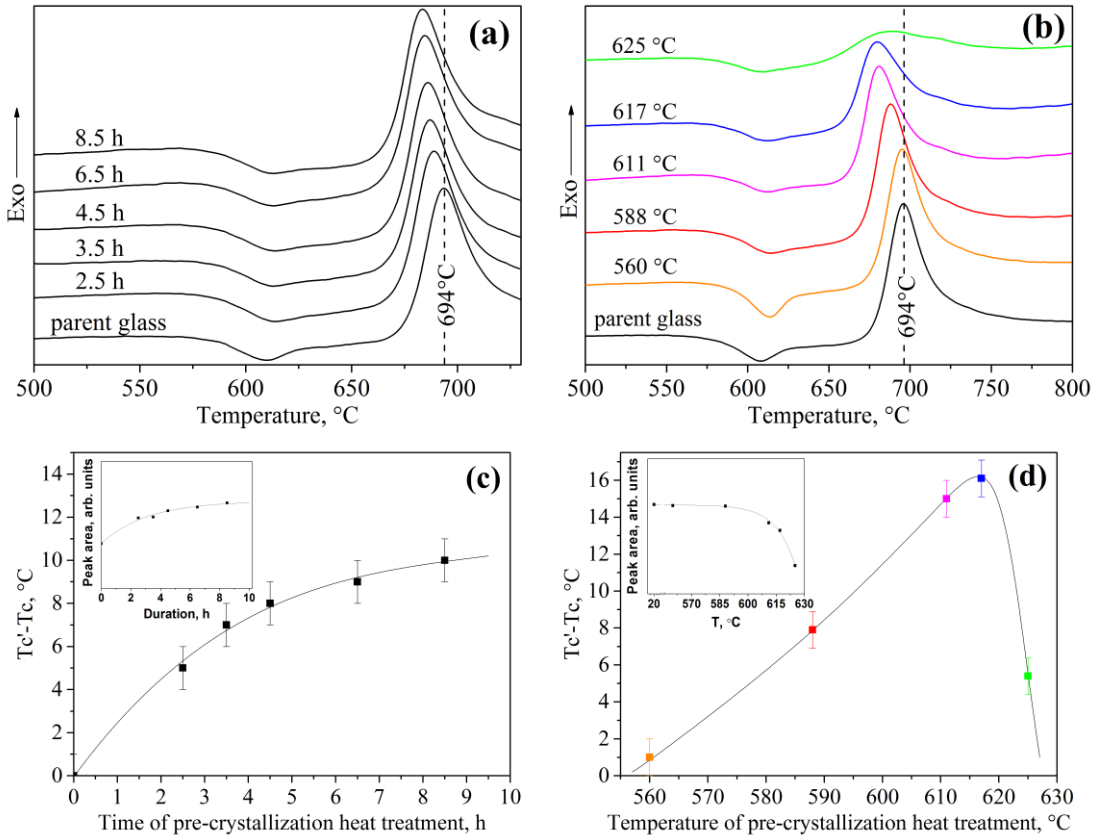

Fig. 1. (a, b) DSC curves (vertically shifted for clarity) of studied glass before (parent) and after pre-crystallization heat treatment at 595 ºC for indicated durations or at indicated temperatures for 3.5 h. (c, d) Shift of the exothermic DSC peak maximum temperature T_c in pretreated samples (with respect to $T_c^{'}$ of the parent glass) vs. time or temperature of pre-crystallization heat treatment. The inserts

show exothermic DSC peak area as a function of pre-crystallization duration and temperature. Curves in (c) and (d) are drawn as a guide to the eyes.

Figure 1a, b shows the DSC curves of the parent glass compared with the glass after pre-crystallization treatment, either at constant temperature (595 ºC) for different time or at different temperatures for fixed duration (3.5 h). The curves register an exothermic crystallization peak at temperature T_c ranging between 680 and 694 ºC. This range is about 100 ºC above T_g (~580 ºC) evidenced by a smooth step. The shift of T_c as a result of pre-crystallization heat treatment is shown in Figure 1c, d. The difference ΔT between peak crystallization temperature in the parent and pretreated glasses grows with the increase of duration of the pre-crystallization heat treatment (Fig. 1c). At the same time, peak area first increases when moving from the DSC curve of the parent glass to the curves of pretreated glasses, then it remains almost unchanged (Fig. 1a, inset in Fig. 1c). By contrast, ΔT vs. pre-treatment temperature shows a maximum (Fig. 1d). In this case, peak area does not practically change up to 588 ºC, then it decreases at higher temperatures (Fig. 1b, inset in Fig. 1d). Such a decrease of glass crystallization indicates that glass is partially crystallized already after pre-treatment above 600 °C, because of the considerable overlap of the nucleation and growth processes at these temperatures. However, the amount of crystallized phase after such pre-treatments turns out to be small and undetectable by XRD. This fact suggests us to call all preliminary heat treatments (with the exception of the treatment at 625 ºC) as pre-crystallization treatment.

3.2 XRD and TEM of parent glass and two-step treated samples

The sub-microstructural effects of pre-crystallization heat treatments on the final nano-crystallization can be extracted from XRD and TEM analyses summarized in Fig. 2 and Fig. 3, respectively. Figure 2 reports some representative XRD results on powdered samples from bulk glass before and after heat treatment for different temperature or treatment duration. A few facts are worth noting. The first fact regards the pattern of the parent glass. Even though it is basically amorphous-like with the usual broad halo observed in glasses, the pattern shows an additional weak and broad

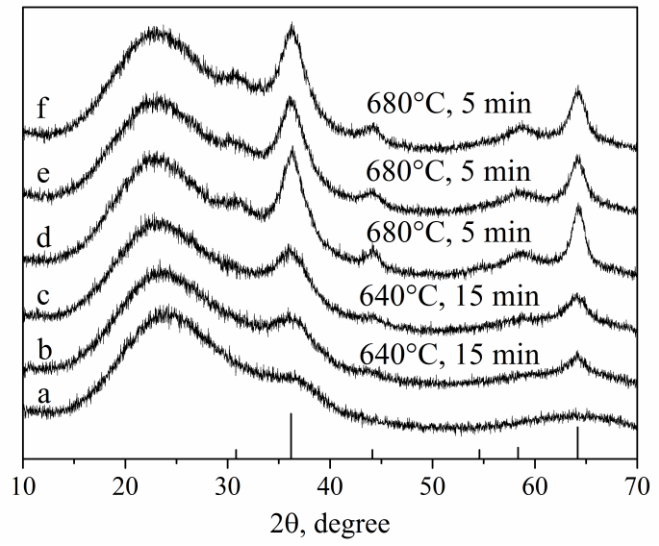

Fig. 2. XRD patterns of the parent glass (a) and the samples treated at indicated conditions without (b, d) and with pre-crystallization heat treatment at 617 (c, e) and 625 ºC (f) for 3.5h. Reflections of γ-Ga_2O_3 phases are indicated by sticks according to PDF file ICDD PDF2 #00-020-0426.

shoulder at around 2θ ~36º, suggesting the occurrence of a sub-micrometer two-phase structure. No evidence of crystalline phases is detected at this stage by TEM: sharp rings are lacking in the diffraction pattern of the parent glass, whereas they are well detectable in heat-treated samples (see insets in Fig. 3a-c). Indeed, amorphous phase separation at the nanometer scale has previously been detected in the glass with the same nominal composition during a small-angle neutron scattering study [30]. Even more drastic phase separation is instead reported in similar but less stable glass compositions of the Li_2O-Ga_2O_3-SiO_2 system. In such a ternary system, crystalline phase already occurs in initial glasses, for instance in $13Li_2O$-$23Ga_2O_3$-$64SiO_2$ and $10Li_2O$-$20Ga_2O_3$-$70SiO_2$ [6, 31], and the lower glass stability makes it difficult melting, drawing a fiber, and controlling optical properties.

The second fact we can highlight regards the occurrence of a set of reflections, ascribable to γ-Ga_2O_3 or $LiGa_5O_8$, as a result of thermal treatments. To better identify the precipitated phase, we treated the parent glass at 680 ºC and have considered the intensity ratio between the diffraction peaks at 2θ = 36.2 and 64.2º (Fig. 2d). From ICDD PDF-2 database, this value is expected to be 2.98 and 1.43 for $LiGa_5O_8$ and γ-Ga_2O_3, respectively. In our case, this ratio is equal to ~1.4 thus suggesting the

precipitation of a spinel γ-Ga_2O_3 phase. The ratio slightly changes, increasing to 1.6, in the glass-ceramics with the highest pre-treatment temperature (Fig. 2f). This result is consistent with the fact that Li ions can diffuse from the glass matrix into γ-Ga_2O_3 NCs to form $LiGa_5O_8$ [32]. Therefore, γ-Ga_2O_3 seems to be the main crystalline phase precipitated in the parent and pretreated glasses after treatment at 640 ºC for 15 min.

The third relevant outcome from XRD analysis is the estimated fraction occupied by the crystal nanophase. The crystallized fraction in the final glass-ceramics, after treatment at 640 ºC for 15 min, results to be different in material obtained from the parent glass and from pretreated (625 ºC, 3.5h) glass, giving values of about 9 and 14 %, respectively.

About the XRD reflections of nanocrystallized gallium oxide, further important indication comes from the careful observation of diffraction peaks width in the XRD patterns. The full width at half maximum $\Delta\theta$ of one-step and two-step treated glasses (Fig. 2d, e) provides evidence of smaller NCs size in samples obtained using pre-crystallization heat treatment. Specifically, taking into account the larger $\Delta\theta$ values in pre-treated samples, the average size d of coherent diffraction domain turns out to be smaller – with a value of about 5 nm – according to Scherrer's equation

$$d = \frac{0.9\lambda}{\cos\theta \cdot \Delta\theta},$$

where λ is the X-ray wavelength and θ is the Bragg angle. No clear effects are instead detected as a function of the pre-crystallization temperature because of the broadness of the XRD pattern. A more detailed and quantitative estimation of the mean size and NCs size distribution is instead provided through the analysis of TEM images (Fig. 3d-i) and is discussed below.

Figure 3 reports TEM images, electron diffraction patterns, and NCs size statistics for representative samples of the investigated materials. The mean size of NCs determined by TEM varies from about 4 to 7 nm and is in reasonable agreement with XRD results. Minor discrepancy is indeed expected, since the analysis of broad XRD reflections and the occurrence of size distribution bring to non-negligible systematic errors in the values estimated by Scherrer's equation. As follows from TEM analysis, the pre-crystallization heat treatment results in decreasing NCs diameter and narrowing size distribution. The smallest NCs size observed in the glass-ceramics pre-treated at 560 and 617 ºC is

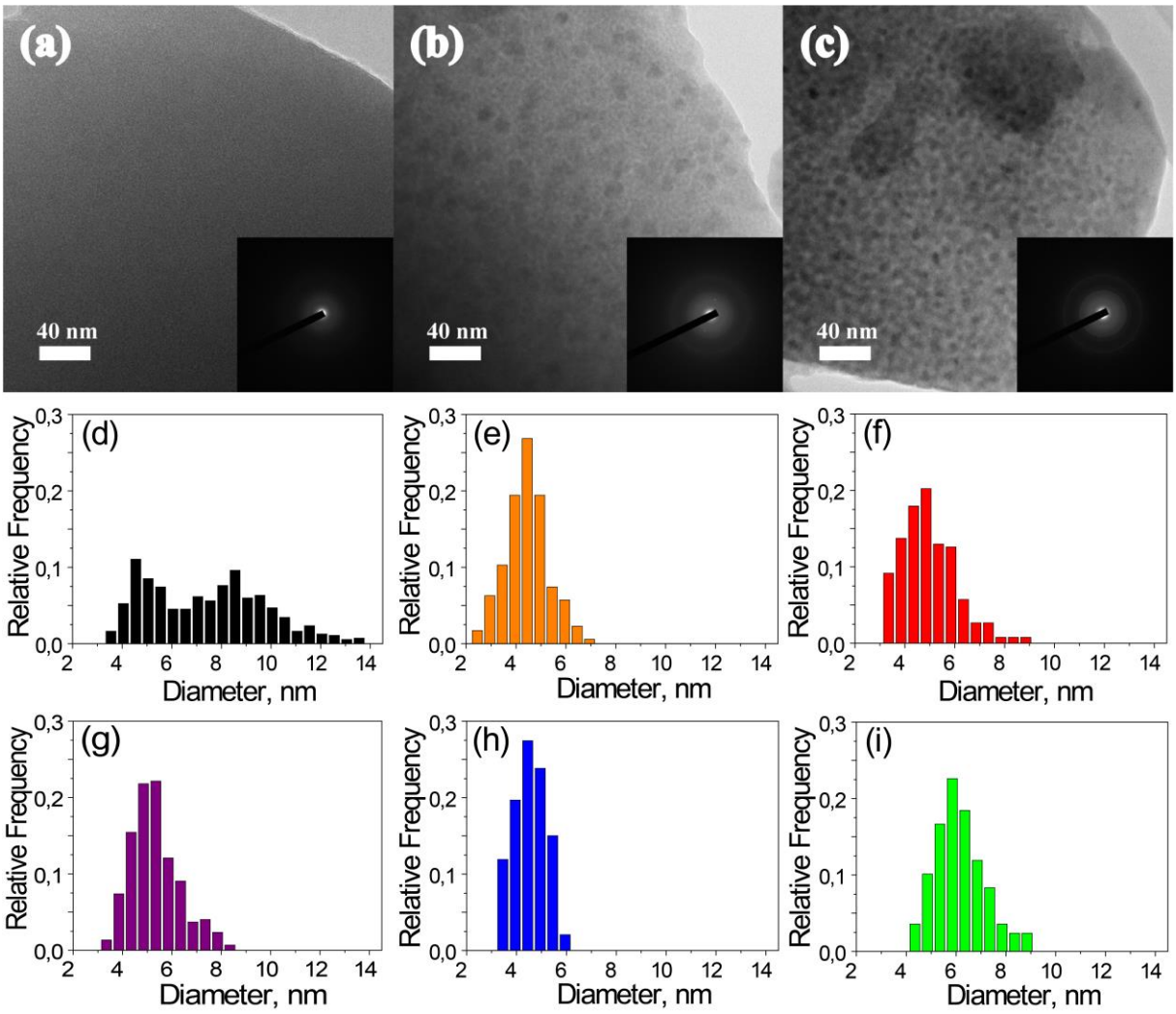

Fig. 3. TEM analysis of the parent glass (a) and the glass-ceramics fabricated using one-step (b, d) and two-step (c, e-i) regime. Transmission electron microscopy images of (a) parent, (b) one-step treated (640 ºC, 15 min) and (c) two-step treated glass (617 ºC, 3.5 h, then 640 ºC, 15 min). The insets are the electron diffraction patterns that were obtained from the same area as corresponding bright-field images. From (d) to (i), histograms of NCs size statistics from the analysis of several TEM images of the samples treated at 640 ºC for 15 min without (d) and after (e-i) pre-crystallization treatment for 3.5 h at 560, 588, 615, 617, and 625 ºC, respectively.

about 4.4 nm. The last temperature lies within the range where the maximum nucleation rate can occur according to DSC data and can be considered as nucleation temperature. The decrease of NCs size in the glass-ceramics pre-treated at 560 ºC is probably due to secondary phase separation [30].

Interestingly, we have found bimodal and broad distribution of NCs size in one-step treated sample. Such a broad distribution, with a relevant tail towards size larger than 10 nm, is one of the reasons of increased light scattering in one-step treated glass-ceramic materials [33]. The occurrence of bigger NCs can be related to the presence of amorphous nano-inhomogeneity regions in the parent glass, with relatively large size (about 8 nm) [30]. This evidence, in fact, suggests the occurrence of NCs directly grown from the native amorphous nano-inhomogeneity regions – already present in the parent glass – with a final size larger than the size of NCs subsequently precipitated in the glass during treatment, as also reported in the work on heat-treated $10Li_2O$-$20Ga_2O_3$-$70SiO_2$ glasses doped with Co^{2+} [31]. In this sense, the bimodal size distribution in one-step treated material indicates a considerable overlapping of the nucleation and growth processes in the studied glass. In regard to two-step treated samples, chemical differentiation into smaller submicroscopic regions during pre-crystallization heat treatments – as we found out in our previous small-angle neutron scattering study [30] – turns out to be the reason for narrowing NCs size distribution.

3.3 Absorption spectra

Thermal treatments drastically alter the visual appearance of the material with respect to the parent glass. The change regards the color, whereas no relevant modification is detected in the attenuation by light scattering, which remains very low despite the formation of NCs (total transmittance is not less than 84% at 1300 nm for ~4 mm samples). The glass color changes from amber to light greenish blue after two-step treatments. Similar but gradual color alteration is also observed in the glass subjected to pre-crystallization heat treatment at temperatures higher than ~ 615 ºC (inset in Fig. 4a). Figure 4 shows some representative optical absorption spectra of the studied samples, including the parent glass, pretreated glasses and glass-ceramics.

Amber coloration of Ni^{2+} bearing silicate glasses is identified as coming from five-fold coordinated Ni^{2+} sites together with a varying proportion of four-fold coordinated ones [34]. According to this attribution, the absorption bands at around 430, 830, 1670 nm and the shoulder at ~510 nm derive from five-folded coordinated Ni^{2+} in trigonal bipyramid, and can be ascribed to the

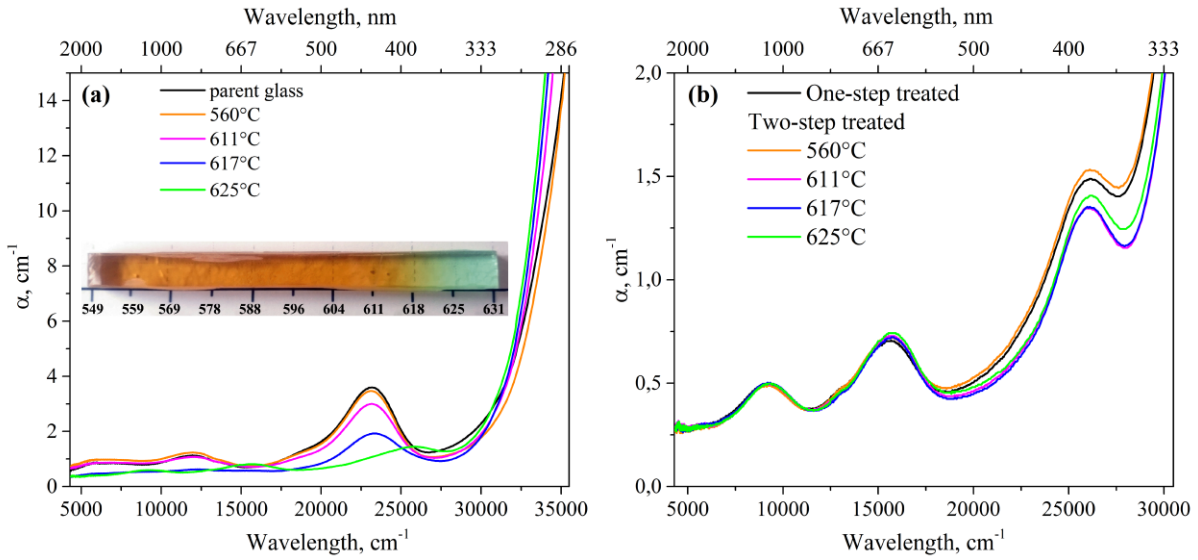

Fig. 4. Optical absorption spectra of 0.1 mol.% Ni^{2+}-doped glass and glass-ceramics: (a) the parent glass and the glasses pretreated for 3.5 h at indicated temperatures; (b) the same glasses after nanocrystallization at 640 ºC for 15 min. Inset: photo of the glass rod treated in the range 550-630 ºC for 3.5 h that was used for sample preparation.

transitions from $^3E'(^3F)$ ground state to $^3A_2'(^3P)$, $^3A_2'(^3F)$ + $^3A_{1(2)}''(^3F)$, $^3E''(^3F)$ and $^3E''(^3P)$ excited states, respectively [35]. Indicator of four-fold coordinated Ni^{2+} is the weak but clearly detectable shoulder at ~730 nm, related to the transition from the ground state $^3T_1(^3F)$ to excited one $^1E(^1D)$ [36]. Therefore, the optical absorption spectra of the parent glass and the glass pretreated at temperatures lower than 617 ºC are predominately determined by five-fold coordinated Ni^{2+} ions located in glass matrix (Fig. 4a). It is interesting to note that some changes in Ni^{2+} environment occur starting even after pre-crystallization treatment at 560 ºC, while the area of the exothermic DSC peak (inset in Fig. 1d) decreases notably only after treatment at 611 ºC. This fact suggests that some rearrangement of the mean coordination environment of Ni^{2+} ions already occurs during the nucleation process and well before the structural rearrangement involved in the crystallization of the gallium oxide nanophase.

The light greenish blue color of heat-treated samples indicates octahedral coordination environment of Ni^{2+} ions. Indeed, the absorption spectra of glass-ceramics (and also the spectrum, not shown, of the glass pretreated at 622 ºC and higher temperature) are very similar to that of Ni^{2+} ions in octahedral sites in other materials [37]. The absorption bands peaking at ~ 380, 640 and 1090 nm can

be attributed to the spin-allowed transitions from the $^3A_{2g}(^3F)$ ground state to $^3T_{1g}(^3P)$, $^3T_{1g}(^3F)$ and $^3T_{2g}(^3F)$ excited states, respectively [35]. The spectral shoulder located around 770 nm can be assigned to the spin-forbidden transition of $^3A_{2g}(^3F) \rightarrow {}^1E_g(^1D)$ [38]. The absorption spectrum of the glass treated at 617 ºC seems to be composed of a combination of five- and six-fold coordinated Ni^{2+} spectra.

The bands in the absorption spectra can be used to extract information about the electronic energy levels and related crystal field parameters. The crystal field strength parameter *Dq* and Racah parameter *B* of octahedral Ni^{2+} in the glass-ceramics are reported in Table I as calculated by using the expressions [39] given by solving the Tanabe-Sugano matrix:

$$Dq = v_1/10$$

$$B = (v_2 - 2v_1)\cdot(v_2 - v_1)/[3\cdot(5v_2 - 9v_1)],$$

where v_1 and v_2 are the wavenumbers corresponding to $^3A_{2g}(^3F) \rightarrow {}^3T_{2g}(^3F)$ and $^3A_{2g}(^3F) \rightarrow {}^3T_{1g}(^3P)$ transitions. The estimated *Dq* value of Ni^{2+} in the glass-ceramics is very close to that in crystals but larger than those in other glasses [39], indicating that Ni^{2+} ions are segregated in the crystal phase of the glass-ceramics. Ni^{2+} ions are supposed to be fully embedded in the γ-Ga_2O_3 NCs, substituting for Ga^{3+} in octahedral spinel sites, as we found out in our previous work by registering the changes of Ni^{2+} optical absorption and NIR luminescence [24].

Table I

Crystal field parameters of studied glass-ceramics after treatment at 640 ºC for 15 min

	Pre-crystallization temperature, ºC										
	-	560	569	578	588	596	604	611	615	617	625
Dq, cm^{-1}	914	918	918	918	917	921	923	926	927	923	929
B, cm^{-1}	920	915	907	903	903	900	901	899	899	907	905

3.4 Photoluminescence of glass-ceramics

No NIR luminescence is detected in the parent glass. By contrast, glass-ceramic materials show a broadband NIR emission between about 1100 and 1600 nm (Fig. 5a). Figure 5a shows some representative PL spectra of the glass-ceramics obtained by one-step and two-step processes, compared with the parent glass. The emission can be attributed to the transition from the $^3T_{2g}(^3F)$ excited state to the $^3A_{2g}(^3F)$ ground state of Ni^{2+} ions in octahedral sites [37]. Figure 5b displays the pre-treatment temperature dependence of the integrated PL intensity, PL lifetime, and amount of crystallized phase. The integrated PL intensity increases with the increase of pre-crystallization temperature and reaches a maximum in the samples pretreated at 615-617 ºC (Fig. 5). PL lifetime follows a somewhat similar behavior, with longer lifetime in almost all double-treated samples than in one-step treated material, and a general increase as a function of pre-treatment temperature from 580 °C to the range 611-625 °C. Importantly, this range roughly matches the temperature range 610-620 ºC of most efficient nucleation registered by DSC analysis.

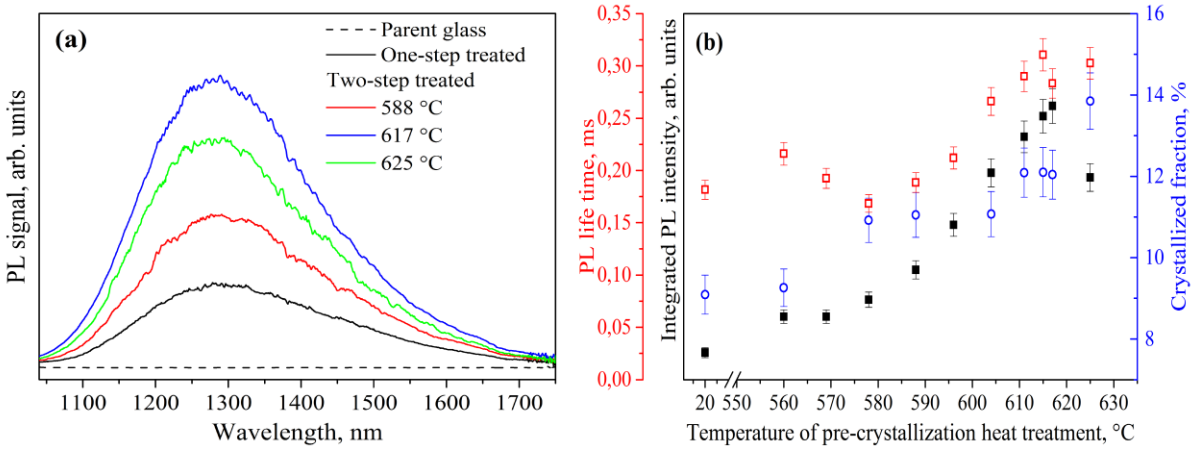

Fig. 5. (a) Photoluminescence spectra of representative samples and (b) integrated intensity of the emission, amount of crystallized phase and mean lifetime as a function of pre-crystallization temperature.

The formation and growth of the crystal nanophase in the final glass-ceramics appears to have an important role on PL, since the increase of crystal fraction is accompanied by larger PL intensity and longer PL lifetime (Fig. 5b). In fact, the larger the total amount of crystal phase, the larger the available space where Ni^{2+} ions are distributed in NCs and, therefore, the lower the active ions mean

density per unit of crystal volume. Such an effect can result in a consequent reduction of concentration quenching of luminescence. At least at a first approximation, a semi-quantitative evaluation of the Ni^{2+} ion concentration per NC can be obtained from the mean NC size and the value of crystalized fraction according to TEM and XRD data, respectively. From these data, in fact, we find (Table II) that the Ni^{2+} ion concentration per NC decreases from ~$4.1 \cdot 10^{20}$ (one-step treated glass) to $2.7 \cdot 10^{20}$ cm^{-3} (glass-ceramics pretreated at 625 ºC) when the PL lifetime increases from about 180 to 300 μs.

However, the increase of crystal fraction alone cannot fully explain all the changes of integrated intensity and PL lifetime along the investigated domain of pre-treatment temperatures. Specifically, starting from the low temperature pre-treatment regime between 560 and 580 °C, the increase of crystal fraction would be expected in a first approximation to slow down the luminescence decay instead of making it faster. Furthermore, we observe that both integrated intensity and lifetime grow in the ranges 578-604 and 611-617 ºC without detectable changes of crystalline fraction. Actually, the error bars are not negligible, and the uncertainty probably hides possible minor changes. Additional mechanisms accompanying the change of crystal fraction seem to play a role in the pre-treatment dependence of PL.

Among the mechanisms that can influence the PL response, we should take in account that a moderate reduction of NC size can cause an increase of interface area and surface defects without a drastic reduction of the number of Ni^{2+} ions per NC, as probably occurs at low pre-treatment temperature (see TEM analysis in Fig. 3e, f, XRD data in Fig. 5b, and Tab. II). In that case, the moderate decrease of concentration quenching of luminescence by lowering the Ni^{2+} concentration per NC is overcome by detrimental effects from non-radiative decay at surface defects. In fact, PL intensity does not increase in Fig. 5b until PL lifetime starts to increase thanks to pre-treatments at temperature closer to the maximum of the nucleation process. When nucleation becomes effective in reducing the NC size (as suggested by TEM analysis) and pre-treatment causes a sensible increase of crystal fraction, the number of NCs sensibly increases and causes a strong reduction of Ni^{2+} ions per NC, which increases the PL efficiency.

An additional mechanism possibly contributing to the observed change of PL features is suggested by the data in Tab. I. The data show that the *Dq* value basically increases as a function of

pre-treatment temperature, somewhat similarly to the behavior of PL lifetime. In fact, if Ni^{2+} ions occupy stronger crystal field sites, the non-radiative rates are smaller that results in longer PL lifetime and more intense PL emission [9]. This observation provides us with an explanation for PL intensity and PL lifetime changes at fixed crystal phase content (and, consequently, fixed Ni^{2+} ion concentration per NC), as registered in the ranges 578-604 and 611-617 ºC. It is worth noting that pre-treatments at temperature immediately higher than the indicated ranges cause noticeable enhancement of PL lifetime, consistently with the occurrence of the concomitant effect of crystal fraction growth and increase of PL yield induced by crystal field enhancement.

In regard to the decrease of integrated PL intensity at the final investigated pre-treatment temperature at 625 °C (while the lifetime does not register relevant change), we notice that such an extreme case requires to take into account possible effects caused by increased light scattering at the highest crystal fraction and the largest size (among two-step treated samples) of NCs, even though not yet evident at a visual inspection. Light scattering turns out to decrease, in fact, both the effective excited volume and the emitted light collection.

Table II

NCs content and Ni^{2+} concentration per NC of representative glass-ceramic samples after treatment at 640 ºC for 15 min

	Pre-crystallization temperature, ºC								
	-	560	578	588	604	611	615	617	625
NCs concentration, 10^{18} cm^{-3} [a]	0.26	1.22	-	1.05	0.83	-	1.15	1.48	0.68
Ni^{2+} concentration per NC, 10^{20} cm^{-3}	4.05	3.97	3.67	3.33	3.32	3.04	3.04	3.06	2.66

[a] Concentration of NCs in cm^{-3} was calculated using density of one-step treated glass-ceramics (3.546 g/cm^{-3}).

4. Conclusion

In summary, we present an effective way to enhance luminescence of glass-ceramics doped with transition metal ions. The method involves the use of pre-crystallization heat treatment to finely tune the sub-microstructure of glass-ceramic material. To test the method, we fabricated optically homogeneous glass and applied two-step treatment to transform it to transparent glass-ceramics. As a result of pre-crystallization heat treatment, the near-infrared luminescence efficiency of Ni^{2+} in the fabricated glass-ceramics is largely increased without losing initial high transparency. The effect can be mainly ascribed to lowering of Ni^{2+} ion concentration per NC and narrowing NCs size distribution as well as to alteration of the crystal field strength of six-fold coordinated Ni^{2+}. The data demonstrate that Ni^{2+} spectroscopy can be notably improved not only by changing the composition of crystalline host in a glass matrix, but also by heat treatment optimization.

Acknowledgements

The work was supported by Mendeleev University of Chemical Technology of Russia. Project Number 023-2018. Financial support from the Italian Ministry of University and Research (MIUR) through grant “Dipartimenti di Eccellenza- 2017 Materials for Energy” is gratefully acknowledged.

References

[1]. V. Marghussian, Nano-Glass Ceramics: Processing, properties and applications, 1st Ed., Elsevier, 2015, 292 p.

[2]. L.R. Pinckney, G.H. Beall, Transition Element-Doped Crystals in Glass, in: A.J. Marker III, M.J. Davis (Eds.), International Society for Optics and Photonics, 2001: pp. 93-99. doi:10.1117/12.446883.

[3]. B.N. Samson, L.R. Pinckney, J. Wang, G.H. Beall, N.F. Borrelli, Nickel-doped nanocrystalline glass-ceramic fiber, Opt. Lett. 27 (2002) 1309. doi:10.1364/OL.27.001309.

[4]. T. Suzuki, G.S. Murugan, Y. Ohishi, Efficient broadband near-infrared emission from Ni^{2+}-doped Li_2O-Ga_2O_3-SiO_2 transparent glass-ceramics, in: (CLEO). Conf. Lasers Electro-Optics, 2005., IEEE, 2005: p. 83-85 Vol. 1. doi:10.1109/CLEO.2005.201684.

[5]. T. Suzuki, G.S. Murugan, Y. Ohishi, Optical properties of transparent Li_2O-Ga_2O_3-SiO_2 glass-ceramics embedding Ni-doped nanocrystals, Appl. Phys. Lett. 86 (2005) 131903. doi:10.1063/1.1891272.

[6]. T. Suzuki, Y. Arai, Y. Ohishi, Crystallization processes of Li_2O-Ga_2O_3-SiO_2-NiO system glasses, J. Non. Cryst. Solids. 353 (2007) 36-43. doi:10.1016/j.jnoncrysol.2006.09.032.

[7]. T. Suzuki, Y. Arai, Y. Ohishi, Quantum efficiencies of near-infrared emission from Ni^{2+}-doped glass-ceramics, J. Lumin. 128 (2008) 603-609. doi:10.1016/j.jlumin.2007.10.010.

[8]. Z. Shi-Feng, F. Gao-Feng, X. Shi-Qing, W. Bo-Tao, Q. Jian-Rong, Broadband Near-Infrared Emission from Transparent Ni^{2+}-Doped Sodium Aluminosilicate Glass Ceramics, Chinese Phys. Lett. 23 (2006) 2996-2998. doi:10.1088/0256-307X/23/11/031.

[9]. S. Zhou, G. Feng, B. Wu, N. Jiang, S. Xu, J. Qiu, Intense infrared luminescence in transparent glass-ceramics containing β-Ga_2O_3:Ni^{2+} nanocrystals, J. Phys. Chem. C. 111 (2007) 7335-7338. doi:10.1021/jp068370i.

[10]. B. Wu, S. Zhou, J. Ren, D. Chen, X. Jiang, C. Zhu, J. Qiu, Broadband infrared luminescence from transparent glass-ceramics containing Ni^{2+}-doped β-Ga_2O_3 nanocrystals, Appl. Phys. B 87 (2007) 697-699. doi:10.1007/s00340-007-2639-1.

[11]. S. Zhou, H. Dong, G. Feng, B. Wu, H. Zeng, J. Qiu, Broadband optical amplification in silicate glass-ceramic containing β-Ga_2O_3:Ni^{2+} nanocrystals, Opt. Express. 15 (2007) 5477. doi:10.1364/OE.15.005477.

[12]. B. Wu, J. Qiu, N. Jiang, S. Zhou, J. Ren, D. Chen, X. Jiang, C. Zhu, Optical properties of transparent alkali gallium silicate glass-ceramics containing Ni^{2+}-doped β-Ga_2O_3 nanocrystals, J. Mater. Res. 22 (2007) 3410-3414. doi:10.1557/JMR.2007.0429.

[13]. S. Zhou, N. Jiang, H. Dong, H. Zeng, J. Hao, J. Qiu, Size-induced crystal field parameter change and tunable infrared luminescence in Ni^{2+}-doped high-gallium nanocrystals embedded glass ceramics, Nanotechnology. 19 (2008) 015702. doi:10.1088/0957-4484/19/01/015702.

[14]. B. Wu, J. Ruan, J. Ren, D. Chen, C. Zhu, S. Zhou, J. Qiu, Enhanced broadband near-infrared luminescence in transparent silicate glass ceramics containing Yb^{3+} ions and Ni^{2+}-doped $LiGa_5O_8$ nanocrystals, Appl. Phys. Lett. 92 (2008) 041110. doi:10.1063/1.2839333.

[15]. J. Luo, B. Wu, B. Zhu, S. Zhou, H. Yang, S. Ye, G. Lakshminarayana, J. Qiu, Energy transfer between Cr^{3+} and Ni^{2+} in transparent glass ceramics containing β-Ga_2O_3 nanocrystals, J. Appl. Phys. 106 (2009) 053527. doi:10.1063/1.3195084.

[16]. B. Wu, J. Qiu, E. Wu, H. Zeng, Brondband near-infrared emission in transparent Ni^{2+}-doped γ-$(Ga,Al)_2O_3$ glass ceramics, in: Adv. Optoelectron. Micro/Nano-Optics, IEEE, 2010: pp. 1-4. doi:10.1109/AOM.2010.5713547.

[17]. S. Zhou, C. Li, G. Yang, G. Bi, B. Xu, Z. Hong, K. Miura, K. Hirao, J. Qiu, Self-Limited Nanocrystallization-Mediated Activation of Semiconductor Nanocrystal in an Amorphous Solid, Adv. Funct. Mater. 23 (2013) 5436-5443. doi:10.1002/adfm.201300969.

[18]. Z. Fang, S. Zheng, W. Peng, H. Zhang, Z. Ma, G. Dong, S. Zhou, D. Chen, J. Qiu, Ni^{2+} doped glass ceramic fiber fabricated by melt-in-tube method and successive heat treatment, Opt. Express 23 (2015) 28258-28263. doi:10.1364/OE.23.028258.

[19]. X. Liu, J. Zhou, S. Zhou, Y. Yue, J. Qiu, Transparent glass-ceramics functionalized by dispersed crystals, Prog. Mater. Sci. 97 (2018) 38-96. doi:10.1016/j.pmatsci.2018.02.006.

[20]. L.R. Pinckney, B.N. Samson, G.H. Beall, J. Wang, N.F. Borrelli, Transparent gallate spinel glass-ceramics, Ceram. Trans. 137 (2003) 265-275. doi:10.13140/2.1.1314.7524.

[21]. N.V. Kuleshova, V.G. Shcherbitsky, V.P. Mikhailov, S. Kück, J. Koetke, K. Petermann, G. Huber, Spectroscopy and excited-state absorption of Ni^{2+}-doped $MgAl_2O_4$, J. Lumin. 71 (1997) 265-268. doi: 10.1016/S0022-2313(96)00284-0.

[22]. R. Ceccato, R.D. Maschio, S. Gialanella, G. Mariotto, M. Montagna, F. Rossi, M. Ferrari, K.E. Lipinska-Kalita, Y. Ohki, Nucleation of Ga_2O_3 nanocrystals in the K_2O-Ga_2O_3-SiO_2 glass system, J. Appl. Phys. 90 (2001) 2522-2527. doi:10.1063/1.1365426.

[23]. N.V Golubev, V.I. Savinkov, E.S. Ignat'eva, S.V Lotarev, P.D. Sarkisov, V.N. Sigaev, L.I. Bulatov, V.M. Mashinskii, V.G. Plotnichenko, E.M. Dianov, Nickel-doped gallium-containing glasses luminescent in the near-infrared spectral range, Glass Phys. Chem. 36 (2010) 657-662. doi:10.1134/S1087659610060039.

[24]. V.N. Sigaev, N. V. Golubev, E.S. Ignat'eva, V.I. Savinkov, M. Campione, R. Lorenzi, F. Meinardi, A. Paleari, Nickel-assisted growth and selective doping of spinel-like gallium oxide

nanocrystals in germano-silicate glasses for infrared broadband light emission, Nanotechnology 23 (2012) 015708. doi:10.1088/0957-4484/23/1/015708.

[25]. A. Paleari, N. V. Golubev, E.S. Ignat'eva, V.N. Sigaev, A. Monguzzi, R. Lorenzi, Donor–Acceptor Control in Grown-in-Glass Gallium Oxide Nanocrystals by Crystallization-driven Heterovalent Doping, ChemPhysChem. (2017). doi:10.1002/cphc.201601247.

[26]. N.V. Golubev, E.S. Ignat'eva, V.N. Sigaev, L. De Trizio, A. Azarbod, A. Paleari, R. Lorenzi, Nucleation-controlled vacancy formation in light-emitting wide-band-gap oxide nanocrystals in glass, J. Mater. Chem. C. 3 (2015) 4380-4387. doi:10.1039/C4TC02837F.

[27]. A. Marotta, S. Saiello, F. Branda, A. Buri, Nucleation and crystal growth in $Na_2O{\cdot}2CaO{\cdot}3SiO_2$ glass: a DTA study, Thermochim. Acta. 46 (1981) 123-129. doi:10.1016/0040-6031(81)80237-7.

[28]. V.M. Fokin, A.A. Cabral, R. M.C.V. Reis, M. L.F. Nascimento, E.D. Zanotto, Critical assessment of DTA–DSC methods for the study of nucleation kinetics in glasses J. Non. Cryst. Solids. 356 (2010) 358-367. doi:10.1016/j.jnoncrysol.2009.11.038.

[29]. V.M. Fokin, E.D. Zanotto, J.W.P. Schmelzer, Homogeneous nucleation versus glass transition temperature of silicate glasses, J. Non. Cryst. Solids. 321 (2003) 52-65. doi:10.1016/S0022-3093(03)00089-9.

[30]. V.N. Sigaev, N.V. Golubev, E.S. Ignat'eva, B. Champagnon, D. Vouagner, E. Nardou, R. Lorenzi, A. Paleari, Native amorphous nanoheterogeneity in gallium germanosilicates as a tool for driving Ga_2O_3 nanocrystal formation in glass for optical devices, Nanoscale. 5 (2013) 299-306. doi:10.1039/C2NR32790B.

[31]. K. Tanaka, T. Mukai, T. Ishihara, K. Hirao, N. Soga, S. Sogo, M. Ashida, R. Kato, Preparation and optical properties of transparent glass-ceramics containing cobalt(II) ions, J. Am. Ceram. Soc. 76 (1993) 2839-2845. doi:10.1111/j.1151-2916.1993.tb04025.x.

[32]. N.V. Golubev, E.S. Ignat'eva, V.N. Sigaev, A. Lauria, L. De Trizio, A. Azarbod, A. Paleari, R. Lorenzi, Diffusion-driven and size-dependent phase changes of gallium oxide nanocrystals in a glassy host, Phys. Chem. Chem. Phys. 17 (2015) 5141-5150. doi:10.1039/C4CP05485G.

[33]. P.A. Tick, Are low-loss glass–ceramic optical waveguides possible?, Opt. Lett. 23 (1998) 1904-1905. doi:10.1364/OL.23.001904.

[34]. L. Galoisy, G. Calas, L. Cormier, B. Marcq, M.H. Thibault, Overview of the environment of Ni in oxide glasses in relation to the glass colouration, in: Phys. Chem. Glasses, 46 (2005): pp. 394-399.

[35]. L. Galoisy, G. Calas, Structural environment of nickel in silicate glass/melt systems: Part I. Spectroscopic determination of coordination states, Geochim. Cosmochim. Acta. 57 (1993) 3613-3626. doi:10.1016/0016-7037(93)90143-K.

[36]. A. Dugué, O. Dymshits, L. Cormier, B. Cochain, G. Lelong, S. Belin, A. Zhilin, Structural evolution of Ni environment in lithium, magnesium and zinc aluminosilicate glasses and glass-ceramics, J. Non. Cryst. Solids. 413 (2015) 24-33. doi:10.1016/j.jnoncrysol.2015.01.011.

[37]. J.F. Donegan, F.J. Bergin, T.J. Glynn, G.F. Imbusch, J.P. Remeika, The optical spectroscopy of $LiGa_5O_8$:Ni^{2+}, J. Lumin. 35 (1986) 57-63. doi:10.1016/0022-2313(86)90008-6.

[38]. P.A. Loiko, O.S. Dymshits, A.A. Zhilin, I.P. Alekseeva, K.V. Yumashev, Influence of NiO on phase transformations and optical properties of $ZnO–Al_2O_3–SiO_2$ glass-ceramics nucleated by TiO_2 and ZrO_2. Part II. Optical absorption and luminescence, J. Non. Cryst. Solids. 376 (2013) 99-105. doi:10.1016/j.jnoncrysol.2013.05.031.

[39]. H. Shigemura, M. Shojiya, R. Kanno, Y. Kawamoto, K. Kadono, M. Takahashi, Optical Property and Local Environment of Ni^{2+} in Fluoride Glasses, J. Phys. Chem. B. 102 (1998) 1920-1925. doi:10.1021/jp973311d.